MethodsX 6 (2019) 1114–1123

Contents lists available at ScienceDirect

MethodsX

journal homepage: www.elsevier.com/locate/mex

Method Article

Synthesis and characterization of porous structures of rutile TiO_2 /$Na_{0.8}Ti_4O_8$/$Na_2Ti_6O_{13}$ for biomedical applications

Diego Fernando Triviño-Bolaños, Rubén Jesús Camargo-Amado*

Escuela de Ingeniería Química, Universidad del Valle, Ciudad Universitaria Meléndez, A. A. 25360 Cali, Colombia

A B S T R A C T

This method involves the use of molding, pressing and sintering techniques applied to different powder mixtures of TiO_2 with sodium bicarbonate $NaHCO_3$ (15 wt% and 30 wt% $NaHCO_3$), to obtain porous structures of rutile TiO_2/$Na_{0.8}Ti_4O_8$/$Na_2Ti_6O_{13}$ and $Na_{0.8}Ti_4O_8$/$Na_2Ti_6O_{13}$ for possible biomedical implant applications. The method validation includes X-ray diffraction patterns (XRD) analysis refined by the Rietveld method using X'Pert HighScore Plus. The surface morphology was observed by using a scanning electron microscopy (SEM) equipped with an energy dispersive spectrometer (EDS), and, finally, a Chinese hamster ovary (CHO) cell line was cultured with the porous structures to determine the effect of material composition on the cellular response using a LDH cytotoxicity assay.

- The method does not require the use of toxic solvents to remove residues.
- The porous structure formed is composed mainly of crystalline phases $Na_2Ti_6O_{13}$/TiO_2 reported as biocompatible.
- It did not need complicated solid-liquid separation processes.

A R T I C L E I N F O

Method name: Synthesis and characterization of porous structures of rutile TiO_2/$Na_{0.8}Ti_4O_8$/$Na_2Ti_6O_{13}$ for biomedical applications

Keywords: Sodium-titanate, Porosity, Crystalline phase

Article history: Received 8 November 2018; Accepted 4 April 2019; Available online 29 April 2019

* Corresponding author.
E-mail address: ruben.camargo@correounivalle.edu.co (R.J. Camargo-Amado).

https://doi.org/10.1016/j.mex.2019.04.002

Specifications Table

Subject area:	Materials Science
More specific subject area:	Nanostructured materials
Method name:	Synthesis and characterization of porous structures of rutile TiO_2/$Na_{0.8}Ti_4O_8$/$Na_2Ti_6O_{13}$ for biomedical applications.
Name and reference of original method:	The most commonly used methods to promote porosity are: slurry foaming, salt leaching, phase separation and lyophilization. Hydrothermal treatment of TiO_2 with NaOH is the method commonly used to obtain sodium titanates.
Resource availability:	N/A

Method details

Overview

In the tissue-engineering field, porous scaffolds must be biocompatible and mechanically stable. Different synthesis methods have been investigated to obtain porous materials for biomedical applications. Among the types of materials used are polymers, such as hydrogels and thermoplastics [1,2], and some types of metals, such as stainless steel [3] and gold [4]. These materials may have limitations due to its composition and synthesis method, including the lack of sufficient biocompatibility with the host, low mechanical stability [5] and, in the case of some metals, insufficient chemical stability in vivo due to the release of toxic ions [6].

Many researchers have studied different synthesis methods such as slurry foaming [7], salt leaching [8], phase separation and lyophilization [9] to promote porosity, but removing undesirable substances generally involve the use of toxic solvents [10,11], which causes cell death when they are not completely eliminated during the process. In this context, ceramic structures such as TiO_2 and sodium titanate have good biocompatibility and chemical stability [12–15].

Regarding to the sodium titanate preparation routes, hydrothermal treatment of TiO_2 with NaOH is the commonly used method, however, this method requires a synthesis time of up to 24 h [16,17], and its result is a precipitation that must be separated by centrifugation and washed with abundant water and ethanol to finally obtain titanate powder [17]. In general, there are still some technological problems involved in the preparation of biocompatible porous structures, requiring several high-cost synthesis methods.

This paper proposes the following method: By applying molding, pressing and sintering techniques in mixtures of TiO_2/$NaHCO_3$ powder materials, it was possible to obtain porous rutile TiO_2/$Na_{0.8}Ti_4O_8$/$Na_2Ti_6O_{13}$ composites (Fig. 1) of the required size and shape, with minimal variations and adequate mechanical properties. Unlike traditional methods, this method does not require the use of toxic solvents to remove residues, because the porous structure formed is mainly composed of crystalline phases of $Na_2Ti_6O_{13}$/TiO_2 reported as biocompatible [14,18] with adequate chemical stability [12–15]. Another advantage of this method was the porosity and roughness control by varying the amount of $NaHCO_3$ and the sintering time [19].

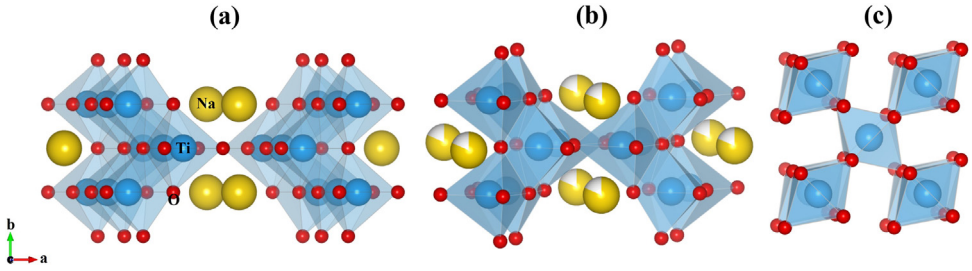

Fig. 1. Crystal structure of (a) $Na_2Ti_6O_{13}$, (b) $Na_{0.8}Ti_4O_8$ and (c) TiO_2 rutile.

At 230 °C the Na_2CO_3 formation (Eq. (1)) responds to a reaction of $NaHCO_3$ at 230 °C [20].

$$2NaHCO_3(s) \overset{230\,^\circ C}{\underset{230\,^\circ C}{C}} Na_2CO_3(s) + CO_2(g) + H_2O(g) \quad (1)$$

Then the solid-state reaction between Na_2CO_3 and TiO_2 (anatase or rutile phase) takes place at temperatures around of 800 °C [21–23]. Na_2CO_3 can also be transformed (Eq. (2)) into Na_2O [24]:

$$Na_2CO_3 \rightarrow Na_2O + CO_2 \quad (2)$$

The release of gases during the heating treatment can promote voids in the structure. Depending on the molar concentration of Na_2O and TiO_2, both can react in the solid state to form different types of sodium titanates according to the binary Na_2O-TiO_2 phase diagram [25]. For a high molar content of TiO_2 (>85 mol%), the main phases formed according to the phase diagram are TiO_2 rutile and $Na_2Ti_6O_{13}$ [22]. Based on the literature, the formation of $Na_2Ti_6O_{13}$ occurs via the decomposition of $Na_2Ti_3O_7$ at temperatures from 400 °C to 1100 °C [15].

In this paper, porous structures of rutile TiO_2/$Na_{0.8}Ti_4O_8$/$Na_2Ti_6O_{13}$ and $Na_{0.8}Ti_4O_8$/$Na_2Ti_6O_{13}$ have been synthesized by molding, pressing and sintering different mixtures of TiO_2/$NaHCO_3$ powder materials. We study the effects of the sintering time and the weight ratio of TiO_2/$NaHCO_3$ on the porosity, and structure proportion of rutile TiO_2 wt%/$Na_{0.8}Ti_4O_8$ wt%/$Na_2Ti_6O_{13}$ wt% and $Na_{0.8}Ti_4O_8$ wt %/$Na_2Ti_6O_{13}$ wt% crystalline phases. Likewise, the biological properties of the materials studied are evaluated in-vitro through cytotoxicity tests with the CHO cell line.

Experimental

Sol-gel synthesis

6 g of TiO_2 were prepared by the sol-gel method. In a typical synthesis, 21 mL of titanium(IV) n-butoxide, 99% (TBT-ACROS) were mixed with 76 mL of absolute ethanol (Aldrich 99.8%) for 10 min under magnetic stirring. Then, 2 mL of deionized distilled water were added at the rate of 1 mL min^{-1} to promote the gelation of the components. The solution was heated at 100 °C for 10 days. Subsequently, the TiO_2 powder was placed inside a muffle furnace (see Fig. 2), heated at the rate of 3.5 °C min^{-1}, sintered at 900 °C for 3 h, and cooled down to 25 °C at the rate of 5 °C min^{-1}.

Mixing and pressing

The TiO_2 and $NaHCO_3$ powders were ball-milled using a Spex Mixer/Mill for 10 min and 2 min respectively. Subsequently, both materials (TiO_2 with 15 wt% $NaHCO_3$; TiO_2 with 30 wt% $NaHCO_3$) were mixed manually. Then, the mixture was poured into a steel mold (13 mm in diameter and approximately 3 mm in height) and pressed uniaxially (35 Kg cm^{-2}) for 5 min using a hydraulic press to form green compacts, as can be seen in Fig. 3.

Fig. 2. TiO_2 powder samples sintered at 900 °C.

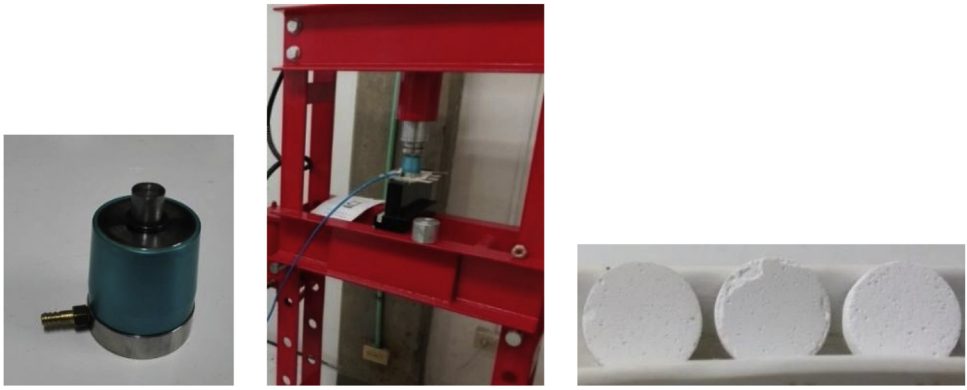

Fig. 3. Mold and uniaxial press used to obtain the green body.

Sintering

After drying at 45 °C for 2 h, the green compact discs were sintered in a tube furnace (Carbolite Gero HTRH) at 1200 °C for 4 h and 8 h in an inert atmosphere (Ar) with a flow rate of 1 L min^{-1} (Fig. 4). The heating rate was 3.5 °C min^{-1} and then cooled to 25 °C at a rate of 5 °C min^{-1}. For all tests, the discs of rutile TiO_2/$Na_{0.8}Ti_4O_8$/$Na_2Ti_6O_{13}$ were polished with 800 and 1200 SiC paper for 2 min each side, and ultrasonically rinsed in acetone for 20 min to remove impurities.

Surface characterization

The characterization of the prepared materials was carried out to validate the formation of rutile TiO_2/$Na_{0.8}Ti_4O_8$/$Na_2Ti_6O_{13}$ and $Na_{0.8}Ti_4O_8$/$Na_2Ti_6O_{13}$ porous structures. XRD patterns were obtained using a Rigaku DMAX 2100 diffractometer; CuK_α radiation (1.54056 Å and 1.54439 Å) was used as an X-ray source in the 2θ range of 20-80°, with a step size of 0.02°.

Identification and quantification of crystalline phases using X'Pert HighScore Plus

Moving forward, the samples prepared under different conditions will be referred to as **T1**: TiO_2 with 15 wt.% of $NaHCO_3$ at 1200 °C for 4 h; **T2**: TiO_2 with 15 wt.% of $NaHCO_3$ at 1200 °C for 8 h, **T3**: TiO_2 with 30% $NaHCO_3$ at 1200 °C for 4 h; and **T4**: TiO_2 with 30 wt.% $NaHCO_3$ at 1200 °C for 8 h.

For the XRD patterns of the materials obtained at conditions T1, T2, T3 and T4, the following methodology was used to identify and quantify three crystalline phases in the materials using the PANalytical X'Pert HighScore Plus software. For the T1 sample, the following analysis procedure was used: Treatment→Search peaks:

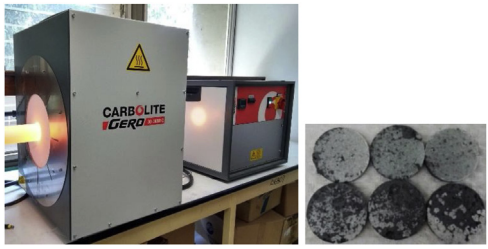

Fig. 4. Sintered disc samples 3 mm thick and 12 mm–13 mm in diameter.

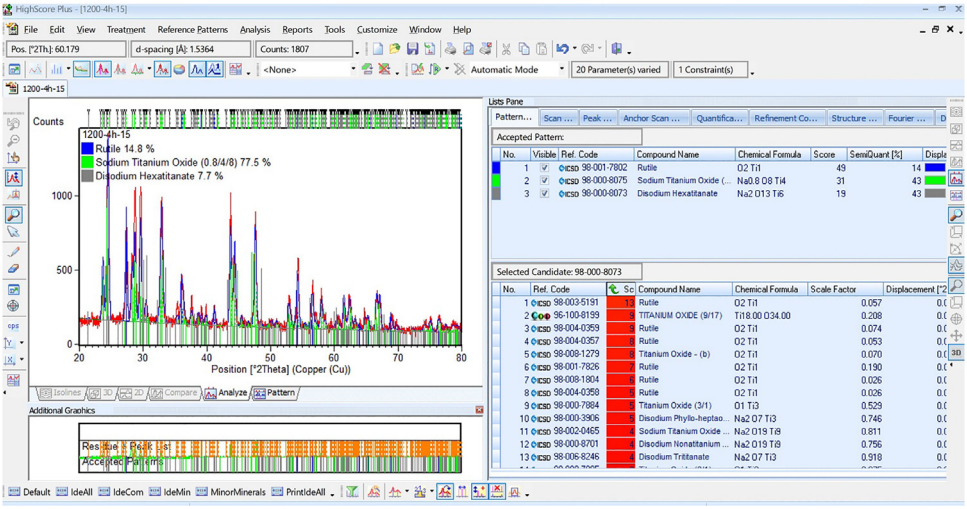

Fig. 5. Refinement results by the Rietveld method using X'Pert HighScore Plus software for sample T1.

Search programming: "Analysis"→ "Search & Match"→ "Execute Search & Match":
Search programming: "Restriction"→ "Edit Restriction Sets"
Search programming: Select possible elements present in the sample(Na, Ti and O):
Select the compounds that most fit the diffractogram
It is also possible to refine the diffractogram by using the Rietveld method to identify the major crystalline phase proportion (wt%) (Fig. 5):

"Analysis" → "Rietveld" → "Star Rietveld Refinement"

Determination of crystallographic orientation

For all samples, it was possible to identify the preferential orientation of the more intense peaks of the crystalline phases. Here are the steps taken: Right click over the refined diffractogram → Label Peaks→Select: n most intense Peaks (for this diffractogram, it is calibrated up to 9). In Labels select: Phase Title and the boxes.

Morphological analysis

The morphology of the materials was characterized using a Phillips ESEM XL30 scanning electron microscope (SEM), operating at 20 kV. The associated energy-dispersive spectrometer (EDS) provided quantitative information about surface elemental composition. The images were obtained at magnifications of 65X and 5000 ×. The pore sizes and surface porosities of the materials were quantified by digital image analysis using ImageJ®

Cytotoxicity test

Cytotoxicity in-vitro tests of 24 h and 48 h were performed using the cytotoxicity Kit LDH [26], which quantifies death and cell lysis based on the measurement of lactate dehydrogenase activity (LDH), released from the cytosol of damaged cells. The biological procedures were carried out in a pre-sterilized laminar flow hood. The working solutions and Kit LDH controls were prepared and applied according to protocol. The LDH release was measured at 24 and 48 h using an Elisa microplate reader (iMark Bio-Rad), with a working length of 492 nm and a reference length of 655 nm.

Results and discussion

The diffraction peaks of the rutile TiO_2, disodium hexatitanate ($Na_2Ti_6O_{13}$) and sodium titanate ($Na_{0.8}Ti_4O_8$) crystalline phases were consistent with the standard patterns (PDF# 98-001-7802, PDF# 98-000-8073 and PDF # 98-000-8075 respectively) and showed tetragonal-monoclinic-monoclinic structures with spatial groups of P 42/m n m, C 2/m, and C 2/m, respectively.

By organizing the data and graphing it in OriginLab® (Fig. 6) for T1, the diffraction peaks at the Bragg angles of 27.4°, 36.1° and 56.5°, are attributed to TiO_2 rutile (110), (101) and (220) crystalline plane respectively. Diffraction peaks (110), (002), (40-1), (310), (003), (60-1), (020), (60-3) and (313) $Na_{0.8}Ti_4O_8$ crystalline planes appeared at 2 θ = 24.5°, 28.7°, 29.7° 32.8°, 43.6°, 44.3° 47.6°, 54.3° and 61.4° respectively.

For T2, the diffraction peaks (110), (101), (210), (211), (220), (002), (310) and (301) TiO_2 rutile planes showed a preferred orientation at 2 θ = 27.3°, 36°, 43.9°, 54.2°, 56.4°, 62.6°, 63.8° and 68.8° respectively. The peaks at around 29.7°, 33.3°, 41.1°, 43.1° and 48.5° are ascribed to $Na_2Ti_6O_{13}$ (310), (402), (511), (603) and (020) planes, respectively. The diffraction peak at around 24.4° is attributed to $Na_{0.8}Ti_4O_8$ (110) crystalline plane.The XRD pattern of T3 exhibited diffraction peaks at around 24.3°, 28.7°, 32.9°, 37.5°, 43.7°, 44.4°, 47.3°, 52.8°, 54.4°, 58° and 61.4° attributed to $Na_{0.8}Ti_4O_8$ (110), (20-2), (310), (401), (003), (60-1), (020), (314), (60-3), (71-1) and (313) crystalline planes respectively. The diffraction peak at around 30.1°, 62.4°, and 66.9° are attributed to $Na_2Ti_6O_{13}$ (20-3), (315) and (62-3) crystalline planes.

In the case of T4, $Na_2Ti_6O_{13}$ showed that its diffraction peaks could be indexed to the (20-3) (30°), (112) (32.2°), (402) (33.4°), (60-1) (35.8°), (511) (41.8°), (60-3) (43.2°), (51-4) (52.6°), (712) (56.1°), (22-3) (58.2°) and (62-3) (67°) planes. Finally, the diffraction peaks at the Bragg angles of 24.3°, 27.2°, 44.3°, 48.5°, 54.3° and 60.2°, are attributed to $Na_{0.8}Ti_4O_8$ (110), (11-1), (60-1), (11-3), (60-3), and (80-1) crystalline planes respectively.

Effects of sintering time and $NaHCO_3$ percentage on the crystalline phases

At T1, the results showed three crystalline phases, in different proportions: 14.8 wt% of rutile TiO_2, 7.7 wt% of $Na_2Ti_6O_{13}$ and 77.5 wt% of $Na_{0.8}Ti_4O_8$, as can be seen in Table 1. The majority phase was sodium titanate or titanium bronze $Na_{0.8}Ti_4O_8$. According to previous research [27], this phase is formed from the reduction of $Na_2Ti_3O_7$ in inert gas atmosphere (hydrogen) at 950 °C for two days. As previously mentioned, the formation of $Na_2Ti_6O_{13}$ also requires the reaction of $Na_2Ti_3O_7$ at temperatures around 400 °C to 1100 °C. However, the $Na_2Ti_3O_7$ phase was not observed in any of the samples analyzed, which suggests that this phase (under reducing atmosphere), can be transformed into $Na_{0.8}Ti_4O_8$ or $Na_2Ti_6O_{13}$.

When comparing the T1 with T2 results, it is observed that in T2, higher concentration of the rutile TiO_2 and $Na_2Ti_6O_{13}$ phases were obtained, while the percentage of $Na_{0.8}Ti_4O_8$ was lower. The main difference between T1 and T2 is the increase of the sintering time from 4 h to 8 h. As the sintering time increases, it is possible that more $Na_2Ti_6O_{13}$ is converted into rutile TiO_2 as it occurs at T2 condition

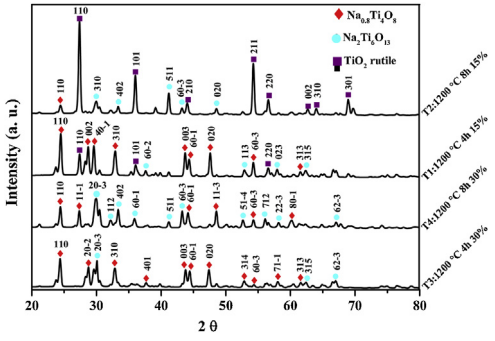

Fig. 6. Diffraction peaks of the TiO_2 rutile, $Na_2Ti_6O_{13}$ and $Na_{0.8}Ti_4O_8$ under T1-T4 condition.

Table 1
Rietveld refinement values from XRD patterns of T1, T2, T3 and T4 samples.

Sample	Phase fraction (wt%)		
	$Na_2Ti_6O_{13}$	$Na_{0.8}Ti_4O_8$	Rutile
T1:1200 °C- 4h-15%	7.7	77.5	14.8
T2:1200 °C-8h-15%	27.7	1.5	70.8
T3:1200 °C-4h-30%	27.6	72.4	–
T4:1200 °C-8h-30%	84.1	15.9	–

[15]. The presence of rutile TiO_2 and $Na_2Ti_6O_{13}$ in the T1 and T2 samples corresponds to Na_2O-TiO_2 phase diagram [25], due to the high mole amounts of TiO_2 (> 85 mol% TiO_2).

While at T3, the proportion of phases obtained was 27.6 wt% of $Na_2Ti_6O_{13}$ and 72.4 wt% of $Na_{0.8}Ti_4O_8$. No rutile TiO_2 peaks were observed in the T3 and T4 samples, probably due to the high content (wt%) of $NaHCO_3$. When comparing this result with the one obtained under condition T4, it was found that the proportion of $Na_2Ti_6O_{13}$ was higher while the proportion of the $Na_{0.8}Ti_4O_8$ phase was lower. It is possible that a sintering time of 8 h promotes higher formation of the $Na_2Ti_6O_{13}$ phase. The main differences between T1-T2 and T3-T4 is the increase on the percentage (wt%) of $NaHCO_3$.

SEM images and EDS pattern

The scanning electron micrographs showed particle sizes with different morphologies (Fig. 7T1 (a)): small spherical particles of 1 μm in diameter and semi-cubic particles of about 3 μm in size. The

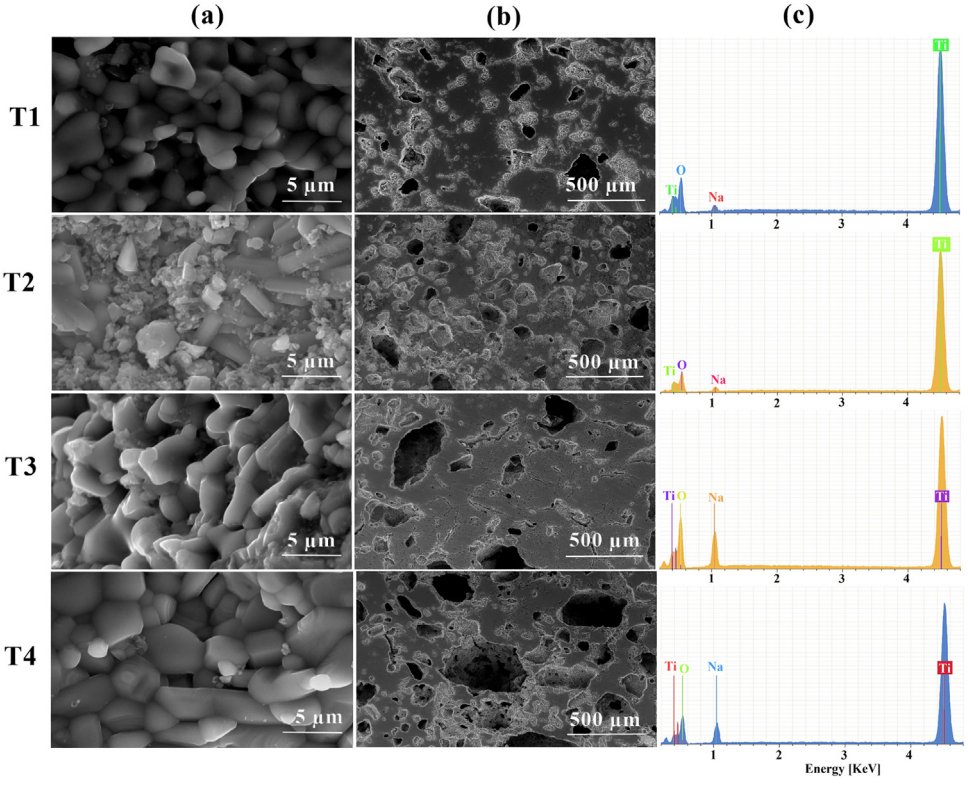

Fig. 7. SEM images of porous structures rutile TiO_2/$Na_{0.8}Ti_4O_8$/$Na_2Ti_6O_{13}$ and $Na_{0.8}Ti_4O_8$/$Na_2Ti_6O_{13}$ at T1, T2, T3 and T4 conditions. (a) 5000X, (b) 65X, (c) EDS analyses of the surface composition.

Table 2
Elemental ratios obtained from EDS results.

Condition	Element	Atomic %	Weight %
T1	O	69.84	44.61
	Na	2.27	2.08
	Ti	27.89	53.31
	Totals	100	100
T2	O	63.75	37.8
	Na	2.32	1.98
	Ti	33.93	60.22
	Totals	100	100
T3	O	68.78	46.83
	Na	9.86	9.65
	Ti	21.36	43.52
	Totals	100	100
T4	O	64.42	40.62
	Na	7.91	7.17
	Ti	27.67	52.21
	Totals	100	100

maximum pore size was 170.5 μm (Fig. 7T1(b)). The grain sized with polygonal structures [28] most probably due to the highest sintering time, is shown in Fig. 7T2(a). Similar results have been reported by other authors [15,22] calcining $Na_2Ti_3O_7$ from 800 °C for several hours. Fig. 7T2(b) exhibited a maximum pore size of 180 μm.

When comparing, the T3(b)-T4(b) samples, showed higher surface porosity than the T1(b)-T2(b) samples. It is possible to observe that the porosity increased as the amount (30 wt%) of $NaHCO_3$ and the sintering time (8 h) increased. In other words, the higher the porogenic percentage and the sintering time, the greater the porosity.

Likewise, it is observed that the grain growth continued with the increase of the sintering time, as can be seen in Fig. 7T2(a) and T4(a). Grain boundaries are evident in the T4(a) sample, demonstrating the good crystallinity and sintering property.

The corresponding elemental composition of the materials is shown in Fig. 7(c), and the elemental ratios as obtained from de EDS detector are presented in Table 2. EDS analysis revealed oxygen, sodium and titanium to be present on the surface.

Depending on the tissue application, appropriate pore sizes can vary from 5 to 500 μm in diameter. For bone tissue engineering applications and designing of macro devices to treat cellular immunodeficiency diseases, the optimal pore diameters vary from 40 to 450 μm [3,29]. In this context, the maximum pore size of the samples obtained at the different treatment conditions were calculated between 50 and 496 μm, which is a widely accepted range for use in biomedical applications.

Cytotoxicity evaluation

The success in the preparation and characterization of any material for use in the biomedical field depends on the positive response that cells, and tissues present upon being in contact with such material once implanted.

The LDH release results at 24 h and 48 h from the CHO cell line showed in Fig. 8. LDH release from all materials in the presence of the cells was low compared to high toxicity control of 1% Triton-X 100

The materials (T3 and T4) with more $NaHCO_3$ (30 wt%) constituted by the $Na_2Ti_6O_{13}$ and $Na_{0.8}Ti_4O_8$ phases caused less LDH release at 24 and 48 h than the materials (T1 and T2) constituted by rutile TiO_2, $Na_2Ti_6O_{13}$ and $Na_{0.8}Ti_4O_8$ phases prepared with less $NaHCO_3$. It is possible that the presence of the rutile phase in the T1 and T2 samples increased the LDH release compared to the materials constituted by $Na_2Ti_6O_{13}$ and $Na_{0.8}Ti_4O_8$ phases. In previous investigations, sodium titanates were prepared via hydrothermal process and sintered at temperatures between 900–1050 °C for 1 h [14]. These materials presented low LDH release in the cytotoxicity assay.

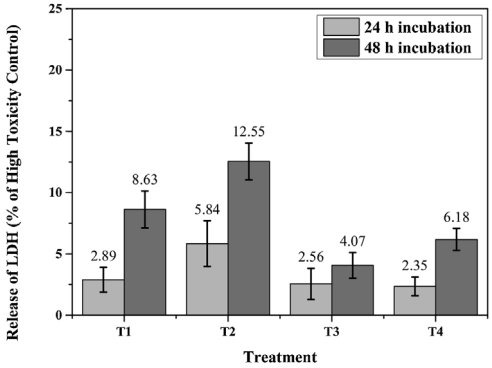

Fig. 8. Results of LDH test after 24 h and 48 h of incubation.

The in-vitro biocompatibility of porous barium titanate manufactured by a direct foaming technique was investigated, using an LDH concentration assay on osteoblast cells cultured for 72 h [29]. In all cases, the results showed that the materials were significantly less toxic to cells, than those cultured with 1% Triton X-100 for 45 min (high toxicity control).

It was demonstrated that the materials evaluated ($TiO_2/Na_{0.8}Ti_4O_8/Na_2Ti_6O_{13}$ and $Na_{0.8}Ti_4O_8/Na_2Ti_6O_{13}$) in the present investigation induce low LDH release (less than 13%).

Conclusion

Porous structures composed of the rutile $TiO_2/Na_{0.8}Ti_4O_8/Na_2Ti_6O_{13}$ and $Na_{0.8}Ti_4O_8/Na_2Ti_6O_{13}$ crystalline phases were obtained by mixing, compacting and sintering TiO_2 with $NaHCO_3$ at different times in an inert Ar atmosphere. It can be concluded that varying these treatment conditions influences the response variables, such as porosity and structure proportion. Moreover, these properties can be controlled to produce a potential suitable material for use in the biomaterials field.

According to the results of the cytotoxicity test, the ceramic porous structures under study induce low LDH release in the presence of the CHO cell line in vitro, regardless of the treatment condition and the rutile $TiO_2/Na_2Ti_6O_{13}/Na_{0.8}Ti_4O_8$ phase fraction, the porous ceramic materials evaluated could be used for biomedical applications. Finally, this method of synthesis could be used for future applications in the biomedical field, replacing conventional manufacturing techniques because of its porous structure and specific crystalline phases that do not affect the in-vitro cell viability.

Acknowledgments

This work was carried out with the financial support of the Universidad del Valle (internal project no. 2838) and the doctoral scholarship Colciencias (no. 528). We are grateful for the X'Pert HighScore Plus 3.0 and VESTA 3.4 software used for qualitative and quantitative identification of crystalline phases and description of their respective atomic models.

References

[1] E.H. Nafea, A. Marson, L. Poole-Warren, P.J. Martens, Immunoisolating semi-permeable membranes for cell encapsulation: focus on hydrogels, J. Control. Release. 154 (2011) 110–122.

[2] J. Kriz, G. Vilk, D.M. Mazzuca, P.M. Toleikis, P.J. Foster, D.J.G. White, A novel technique for the transplantation of pancreatic islets within a vascularized device into the greater omentum to achieve insulin independence, Am. J. Surg. 203 (2012) 793–797.

[3] A. Pileggi, R.D. Molano, C. Ricordi, E. Zahr, J. Collins, R. Valdes, L. Inverardi, Reversal of diabetes by pancreatic islet transplantation into a subcutaneous, neovascularized device, Transplantation. 81 (2006) 1318–1324.

[4] C.L. Randall, Y.V. Kalinin, M. Jamal, A. Shah, D.H. Gracias, Self-folding immunoprotective cell encapsulation devices, Nanomed. Nanotechnol. Biol. Med. 7 (2011) 686–689.
[5] A.M. a Rokstad, I. Lacík, P. de Vos, B.L. Strand, Advances in biocompatibility and physico-chemical characterization of microspheres for cell encapsulation, Adv. Drug Deliv. Rev. 67-68 (2013) 111–113.
[6] E.B. Taddei, V.A.R. Henriques, C.R.M. Silva, C.A.A. Cairo, Production of new titanium alloy for orthopedic implants, Mater. Sci. Eng. C. 24 (2004) 683–687.
[7] H.C. Hsu, S.-K. Hsu, S.-C. Wu, P.H. Wang, W.F. Ho, Design and characterization of highly porous titanium foams with bioactive surface sintering in air, J. Alloys Compd. 575 (2013) 326–332.
[8] P. Bartolo, J.P. Kruth, J. Silva, G. Levy, A. Malshe, K. Rajurkar, M. Mitsuishi, J. Ciurana, M. Leu, Biomedical production of implants by additive electro-chemical and physical processes, CIRP Ann. Manuf. Technol. 61 (2012) 635–655.
[9] L. Ren, Y.-P. Zeng, D. Jiang, Preparation of porous TiO_2 by a novel freeze casting, Ceram. Int. 35 (2009) 1267–1270.
[10] V. Iacovacci, L. Ricotti, A. Menciassi, P. Dario, The bioartificial pancreas (BAP): biological, chemical and engineering challenges, Biochem. Pharmacol. 100 (2016) 12–27.
[11] D.W. Hutmacher, Scaffolds in tissue engineering bone and cartilage, Biomaterials 21 (2000) 2529–2543.
[12] Z. Minjing, L. Gang, W. Qiang, C. Hualei, L. Ling, Preparation of porous TiO_2/Ti composite membrane for immunoisolation, Appl. Surf. Sci. 255 (2008) 2256–2258.
[13] N. Ohtsu, S. Semboshi, C. Abe, S. Tokuda, Fabrication of composite coating comprising bioactive calcium and sodium titanates on titanium using calcium hydroxide slurry containing sodium ions, Surf. Coat. Technol. 205 (2011) 3785–3790.
[14] Y. Shen, Z. Hua, L. Zhang, X. Hao, Bioglass-assisted preparation of network sodium titanate bioceramics, RSC Adv. 5 (2015) 18788–18795.
[15] A.L. Sauvet, S. Baliteau, C. Lopez, P. Fabry, Synthesis and characterization of sodium titanates $Na_2Ti_3O_7$ and $Na_2Ti_6O_{13}$, J. Solid State Chem. 177 (2004) 4508–4515.
[16] D.R. Zhang, C.W. Kim, Y.S. Kang, A study on the crystalline structure of sodium titanate nanobelts prepared by the hydrothermal method, J. Phys. Chem. C 114 (2010) 8294–8301.
[17] Y. Zhang, H. Hou, X. Yang, J. Chen, M. Jing, Z. Wu, X. Jia, X. Ji, Sodium titanate cuboid as advanced anode material for sodium ion batteries, J. Power Sources 305 (2016) 200–208.
[18] L. Zhao, J. Chang, W. Zhai, Effect of crystallographic phases of TiO_2 on hepatocyte attachment, proliferation and morphology, J. Biomater. Appl. 19 (2005) 237–252.
[19] A. Carradò, F. Perrin-Schmitt, Q.V. Le, M. Giraudel, C. Fischer, G. Koenig, L. Jacomine, L. Behr, A. Chalom, L. Fiette, A. Morlet, G. Pourroy, Nanoporous hydroxyapatite/sodium titanate bilayer on titanium implants for improved osteointegration, Dent. Mater. 33 (2017) 321–332.
[20] M. Hartman, K. Svoboda, M. Pohořelý, M. Šyc, Thermal decomposition of sodium hydrogen carbonate and textural features of its calcines, Ind. Eng. Chem. Res. 52 (2013) 10619–10626.
[21] S. Baliteau, A.L. Sauvet, C. Lopez, P. Fabry, Controlled synthesis and characterization of sodium titanate composites $Na_2Ti_3O_7$/$Na_2Ti_6O_{13}$, Solid State Ionics 178 (2007) 1517–1522.
[22] I. Becker, I. Hofmann, F.A. Müller, Preparation of bioactive sodium titanate ceramics, J. Eur. Ceram. Soc. 27 (2007) 4547–4553.
[23] J. Ramírez-Salgado, E. Djurado, P. Fabry, Synthesis of sodium titanate composites by sol-gel method for use in gas potentiometric sensors, J. Eur. Ceram. Soc. 24 (2004) 2477–2483.
[24] S. Papp, L. Kőrösi, V. Meynen, P. Cool, E.F. Vansant, I. Dékány, The influence of temperature on the structural behaviour of sodium tri- and hexa-titanates and their protonated forms, J. Solid State Chem. 178 (2005) 1614–1619.
[25] R. Bouaziz, M. Mayer, The binary sodium oxide-titanium dioxide, C. R. Hebd. Seances Acad. Sci. 272 (1971) 1874–1877.
[26] Manual, Cytotoxicity Detection Kit (LDH), E-Labdoc.Roche.Com., (2012) , pp. 1–20.
[27] S. Andersson, D. Wadsley, $Na_xTi_4O_8$ an alkali metal titanium dioxide bronze, Acta Crystallogr. 15 (1962) 201–206.
[28] R. Singh, P.D. Lee, J.R. Jones, G. Poologasundarampillai, T. Post, T.C. Lindley, R.J. Dashwood, Hierarchically structured titanium foams for tissue scaffold applications, Acta Biomater. 6 (2010) 4596–4604.
[29] J.P. Ball, B.A. Mound, J.C. Nino, J.B. Allen, Biocompatible evaluation of barium titanate foamed ceramic structures for orthopedic applications, J. Biomed. Mater. Res. - Part A. 102 (2014) 2089–2095.